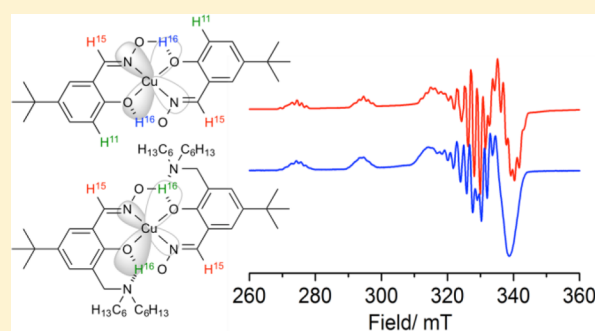


## EPR/ENDOR and Computational Study of Outer Sphere Interactions in Copper Complexes of Phenolic Oximes

Mary R. Healy,<sup>†</sup> Emma Carter,<sup>‡</sup> Ian A. Fallis,<sup>‡</sup> Ross S. Forgan,<sup>†</sup> Ross J. Gordon,<sup>†</sup> Eduardo Kamenetzky,<sup>§</sup> Jason B. Love,<sup>†</sup> Carole A. Morrison,<sup>†</sup> Damien M. Murphy,<sup>\*,‡</sup> and Peter A. Tasker<sup>\*,†</sup><sup>†</sup>EaStCHEM School of Chemistry, University of Edinburgh, Edinburgh, EH9 EJJ, United Kingdom<sup>‡</sup>School of Chemistry, Cardiff University, Park Place, Cardiff, CF10 3AT, United Kingdom<sup>§</sup>Cytec Industries, 1937 West Main Street, Stamford, Connecticut 06904-0060, United States

## Supporting Information

**ABSTRACT:** Copper complexes of the phenolic oxime family of ligands (3-X-salicylaloximes) are used extensively as metal solvent extractants. Incorporation of electronegative substituents in the 3-position, ortho to the phenol group, can be used to buttress the interligand H-bonding, leading to an enhancement in extractant strength. However, investigation of the relevant H-bonding in these complexes can be exceedingly difficult. Here, we have combined EPR, ENDOR, DFT, and X-ray crystallography to study this effect. Analysis of the <sup>1</sup>H ENDOR data revealed a variation in the Cu···H<sup>16</sup> (oxime proton) distance from 2.92 Å for the unsubstituted complex [Cu(L<sup>2</sup>)<sub>2</sub>] to 3.65 Å for the X = CH<sub>2</sub>N(C<sub>6</sub>H<sub>13</sub>)<sub>2</sub> substituted complex [Cu(L<sup>3</sup>)<sub>2</sub>]. DFT calculations showed that this variation is caused by changes to the length and strength of the H-bond between the oximic hydrogen and the phenolate oxygen. Noticeable changes to the Cu···H<sup>15</sup> (azomethine proton) distances and the Cu···N bonding parameters were also observed in the two complexes, as revealed through the <sup>N</sup>A and <sup>N</sup>Q ENDOR data. Distortions in the structure of the complex and variations in the oximic proton to phenolate oxygen H-bond strength caused by the substituent (X) were confirmed by DFT and X-ray crystallography. DFT directly evidenced the importance of the interaction between H<sup>16</sup> and the amine nitrogen of CH<sub>2</sub>N(C<sub>6</sub>H<sub>13</sub>)<sub>2</sub> in the buttressed complex and indicated that the high strength of this interaction may not necessarily lead to an enhancement of copper extraction, as it can impose an unfavorable geometry in the inner coordination sphere of the complex. Therefore, ENDOR, DFT, and X-ray structural data all indicate that the aminomethyl substituent (X) ortho to the phenolic oxygen atom provides a particularly strong buttressing of interligand H-bonding in these copper complexes and that these outer sphere interactions can significantly influence structure and stability.



## INTRODUCTION

The interaction between ligands in the outer coordination spheres of metal ions often contributes to the thermodynamic and kinetic stability of the complexes in systems as diverse as antibiotics,<sup>1</sup> gravimetric reagents,<sup>2</sup> and metal solvent extractants.<sup>3a,b</sup> The last are used in kilotonne-scale processes in extractive metallurgy and provide very efficient ways to achieve the necessary operations for the concentration and separation of metals dissolved in an aqueous acidic solution by selective transfer into an organic phase.<sup>4</sup> The hydrogen-bonding (H-bonding) interactions of metal complexes,<sup>5</sup> particularly those between ligands, is favored in the high-boiling nonpolar solvents used by industry for metal solvent extraction and are often responsible for the selectivity of extraction, which is essential for efficient recovery processes. Metal extraction by organic derivatives of phosphorus(V) acids, such as the commercially used reagent di-(2-ethylhexyl)phosphoric acid (D2EHPA), is usually associated with retention of strong interligand H-bonds and the formation of eight-membered

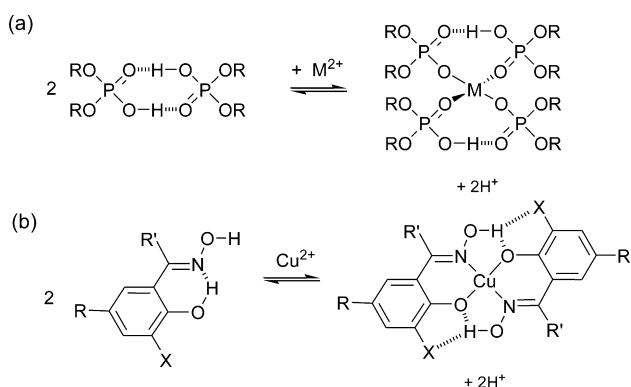
pseudochelate rings (Scheme 1a),<sup>4b</sup> favoring complex formation with tetrahedral metal cations and leading to selectivity for Zn(II) over other first-row transition metal(II) cations. This selectivity is now exploited in a zinc-plant in Namibia that operates on a 150 000 tonne per annum scale.<sup>6</sup>

Interligand H-bonding is also important in determining the extraction strength and selectivity of the phenolic oxime reagents (Scheme 1b) used in copper recovery,<sup>7</sup> which now account for between 20 and 30% of the world's production of copper.<sup>8</sup> The incorporation of electronegative substituents (X) in the 3-position, ortho to the phenol group (Scheme 1b), can be used to buttress the interligand H-bonding and leads to substantial increases in extractant strength.<sup>9</sup> The relative strengths of pH-swing extractants of the types shown in Scheme 1 are usually evaluated by comparing their pH<sub>0.5</sub> values (the pH observed for 50% metal loading in experiments

Received: May 25, 2015

Published: August 19, 2015

**Scheme 1. Two pH-Swing Extractants That Form Interligand H-Bonds<sup>a</sup>**



<sup>a</sup>(a) Phosphoric acid diesters (e.g., D2EHPA, R = 2-ethylhexyl) used in zinc recovery<sup>6</sup> and (b) 5-alkyl-substituted salicylaldoximes (R' = X = H) used in copper recovery.<sup>7</sup>

determining metal uptake as a function of the pH of the aqueous phase at equilibrium; see, for example, Figure 6).

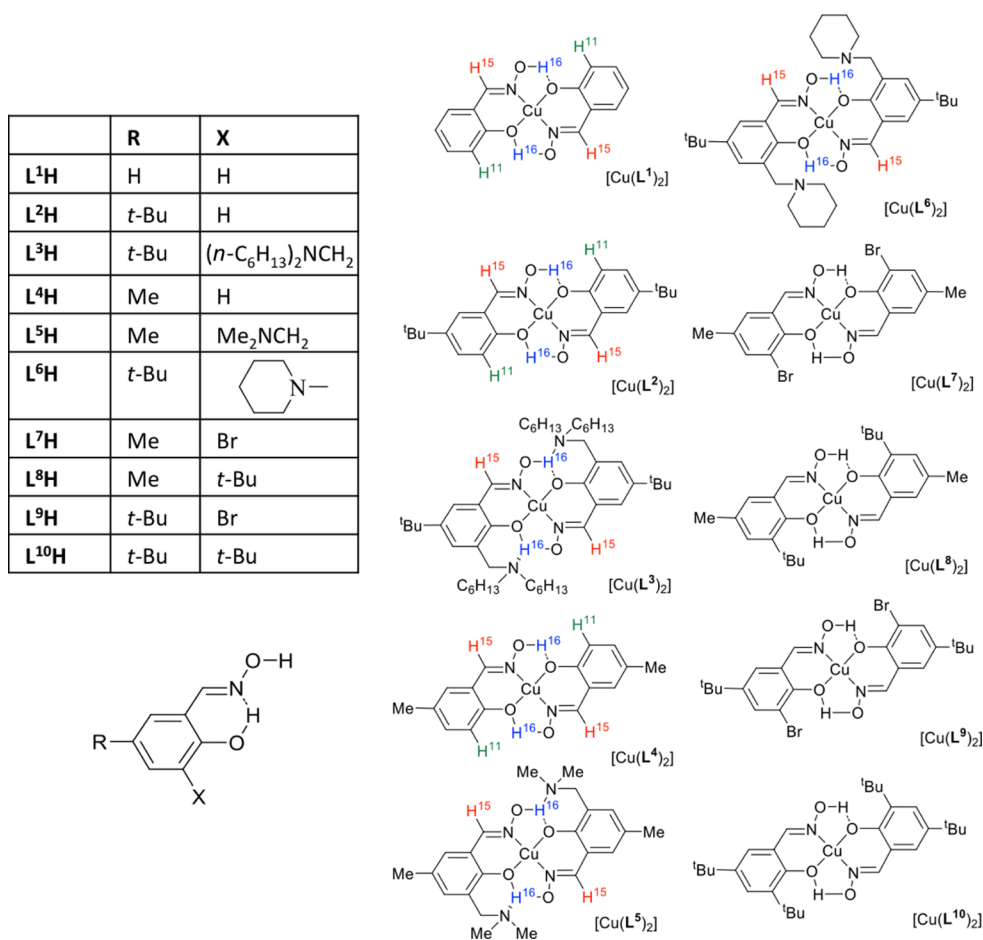
Structural information on copper complexes of the phenolic oximes in the regions that form the interligand H-bonds is important for understanding the origins of such buttressing effects but is difficult to obtain. The precision with which H atoms can be located in transition metal complexes by X-ray

structure determination is limited, and, in the solid state, Cu cations have a propensity to form weak bonds to donor atoms in neighboring molecules, which, in turn, influences the Cu–O and Cu–N bond lengths in the cavity of the molecule and changes the interligand contact distances.<sup>10</sup> In order to replicate the conditions that apply in solvent extraction, it is preferable to probe the structures of the complexes in solution. Fortunately, the paramagnetism of Cu(II) enables the systems to be readily characterized using EPR techniques; therefore, in this Article, we have utilized a combination of continuous wave (CW) electron paramagnetic resonance (EPR) and electron nuclear double resonance (ENDOR) spectroscopy, supported by computational methods, to determine the variation in Cu...<sup>1</sup>H distances as a function of changes in the outer coordination sphere of some of the compounds shown in Scheme 2. The predicted strengths of the hydrogen bonds and differences in the copper coordination spheres are discussed within the context of experimental structures, solvent extractions, and X-ray structures.

## EXPERIMENTAL SECTION

The syntheses of the *t*-butyl-substituted proligands L<sup>2</sup>H, L<sup>3</sup>H, L<sup>6</sup>H, L<sup>9</sup>H, and L<sup>10</sup>H (Scheme 2) used in the experimental work and the associated preparation and characterization, including X-ray structure determinations of their copper complexes, have been reported previously.<sup>9,11</sup> The other proligands in Scheme 2 were used only in computational work. The solvent extraction of copper by proligands

**Scheme 2. Structures of the Complexes and the Labeling Used to Define the Hydrogen Atoms of the Azomethine (H<sup>15</sup>) and Oxime (H<sup>16</sup>) Groups and in the 3-Phenyl Position (H<sup>11</sup>) of [Cu(L<sup>i</sup>)<sub>2</sub>]**



$L^2H$ ,  $L^3H$ ,  $L^9H$ , and  $L^{10}H$  (Figure 6) has also been reported previously.<sup>9,10</sup>

**EPR/ENDOR Spectroscopy.** Dilute solutions of  $[Cu(L^2)_2]$  and  $[Cu(L^3)_2]$  were prepared by dissolving the compounds in a 1:1 toluene/dichloromethane solvent. The X-band (9 GHz) CW-EPR spectra were recorded at 140 K on a Bruker EMX spectrometer operating at 100 kHz field modulation, 10 mW microwave power using an ER 4119HS cavity. Q-band (35 GHz) CW-EPR and ENDOR spectra were recorded on a Bruker ESP 300E series spectrometer equipped with an ESP360 DICE ENDOR unit operating at 12.5 kHz field modulation in a Q-band ENDOR cavity (Bruker ER 5106 QT-E). The ENDOR spectra were obtained using 8 dB RF power from an ENI A-300 RF amplifier and 50 or 200 kHz RF modulation depth and 1 mW microwave power. Q-band EPR spectra were recorded at 50 K, and the Q-band ENDOR measurements were performed at 10 K. Spectral simulations were performed using the EasySpin toolbox in Matlab developed at ETH Zurich.<sup>12</sup>

**Computations.** All calculations were executed using the Gaussian '09 program.<sup>13</sup> Full structural optimizations and NBO 6.0<sup>14</sup> analyses were carried out using the hybrid DFT functional B3LYP,<sup>15</sup> coupled to the 6-31+G(d,p) basis set for each of the proligands, proligand dimers, and copper complexes. Vibrational frequency calculations were carried out on all optimized structures to ensure that energy minima had been reached. Assembly formation energies and dimerization and deprotonation energies were calculated using the difference in internal energy values based on the sum of the products and the sum of individual reactants. A correction factor for basis set superposition error (BSSE) was also included, which was determined using the counterpoise method of Boys and Bernardi.<sup>16</sup>

## RESULTS AND DISCUSSION

$L^1H$  represents the unsubstituted proligand. The  $[Cu(L^1)_2]$  complex (Scheme 2) was studied several years ago using ENDOR spectroscopy by Schweiger as a doped single crystal and solid solution using the isomorphous  $[Ni(L^1)_2]$  complex.<sup>17–19</sup> The *t*-butyl and additional *n*-hexyl groups in  $L^2H$  and  $L^3H$ , respectively, provide sufficient solubility in nonpolar solvents to allow extraction experiments to be carried out and for these solutions to be subsequently characterized by EPR and ENDOR spectroscopy. Methyl substituents were used in the DFT calculations (labeled  $L^4H$ ,  $L^5H$ ,  $L^7H$ , and  $L^8H$ ; Scheme 2) to reduce the number of conformers in the side chains when defining energy-minimized forms, whereas the restricted flexibility of the piperidine group in  $L^6H$  permitted the isolation of single crystals of  $[Cu(L^6)_2]$  suitable for X-ray structure determination.<sup>11</sup> It is worth noting that commercial extractants normally carry branched mixed isomer nonyl or dodecyl groups in the 5-position to impart solubility in kerosene organic phases. The EPR spectra of copper complexes bearing such commercial extractants have been reported previously, providing evidence that 2:1 complexes of the type shown in Scheme 2 are formed in hydrocarbon solvents and that adducts can be formed with strongly basic ligands such as ammonia or pyridine.<sup>20</sup>

**X- and Q-Band EPR.** Low-temperature frozen solution (140 or 50 K) CW EPR measurements of  $[Cu(L^2)_2]$  and  $[Cu(L^3)_2]$  were undertaken at both X- and Q-band frequencies. The resulting spectra are shown in Figure 1. The well-resolved X-band EPR spectra contain a large number of lines arising from the superhyperfine interactions to neighboring ligand nuclei ( $^{14}N$ ,  $^1H$ ), and the spectra are further complicated by the presence of additional features arising from angular anomalies. These anomalies occur because, to first order, the hyperfine splittings remain equal at any given orientation of the applied field with respect to the  $g$  frame;<sup>21,22</sup> the relative anisotropy of  $g$  and  $^{63}Cu$  in any plane will then determine whether additional

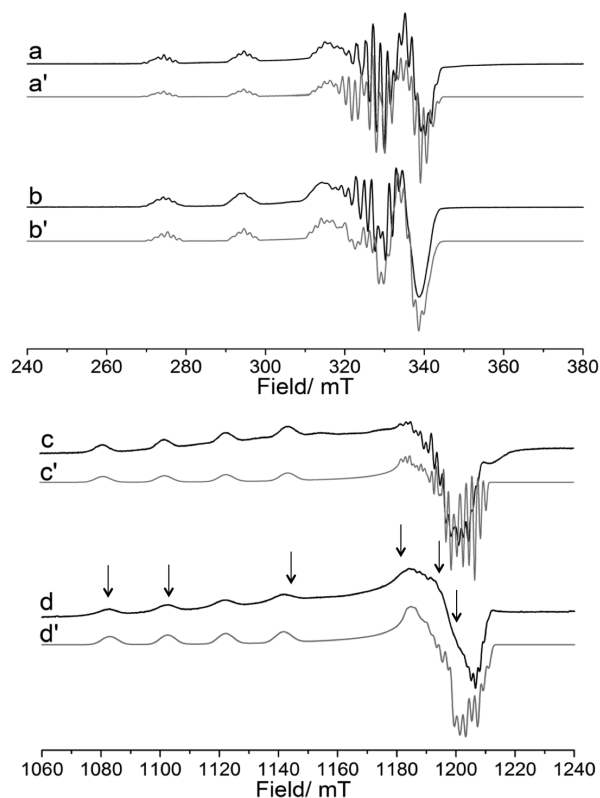


**Figure 1.** X-band CW EPR spectra (140 K) of (a)  $[Cu(L^2)_2]$  and (b)  $[Cu(L^3)_2]$ . The corresponding simulations are shown in a' and b'. The corresponding Q-band CW EPR spectra (50 K) are shown in (c) and (d). The field positions used for the ENDOR measurements are marked with an arrow.

turning directions will occur for orientations away from the principal or canonical directions. The effects are usually observed in Cu(II) systems with relatively large anisotropy in the principal  $g$  values, combined with substantial hyperfine splittings in the perpendicular region of the spectrum, but they are easily resolved by measurements at higher frequencies (Q-band).

A solid-state EPR and ENDOR investigation of the closely related  $[Cu(L^1)_2]$  complex (Scheme 2) was originally reported by Schweiger.<sup>17–19</sup> The principal values of the  $g$  and  $^{63}Cu$  tensors for  $[Cu(L^1)_2]$  are given in Table 1, where a slight rhombic distortion in  $g$  can be noted. These reported  $g/A$  values were used as a starting point to simulate the frozen solution X- and Q-band EPR spectra of  $[Cu(L^2)_2]$  and  $[Cu(L^3)_2]$  (Figure 1). The agreement between the single crystal/solid solution data for  $[Cu(L^1)_2]$ <sup>17–19</sup> and the frozen

**Table 1.**  $g$  and  $^{63}Cu$  Spin Hamiltonian Parameters for  $[Cu(L^1)_2]$ ,  $[Cu(L^2)_2]$ , and  $[Cu(L^3)_2]$ <sup>a</sup>

|               | $g_x^b$ | $g_y^b$ | $g_z^c$ | $A_x^d$ | $A_y^d$ | $A_z^e$ | ref       |
|---------------|---------|---------|---------|---------|---------|---------|-----------|
| $[Cu(L^1)_2]$ | 2.056   | 2.039   | 2.203   | -109    | -111    | -609    | 17        |
| $[Cu(L^2)_2]$ | 2.056   | 2.039   | 2.20    | -109    | -111    | -640    | this work |
| $[Cu(L^3)_2]$ | 2.050   | 2.039   | 2.20    | -109    | -111    | -620    | this work |

<sup>a</sup>The  $[Cu(L^2)_2]$  and  $[Cu(L^3)_2]$  samples were dissolved in a 1:1 toluene/dichloromethane mixture. All  $A_i$  values are reported in MHz. <sup>b</sup> $\pm 0.003$ . <sup>c</sup> $\pm 0.003$ . <sup>d</sup> $\pm 5$ . <sup>e</sup> $\pm 3$ ; the sign of  $A_i$  was determined with reference to the single-crystal work of  $[Cu(L^1)_2]$ .

solution data presented here is excellent; a small difference is noted in the  $A_z$  ( $A_{\parallel}$ ) component of the  $^{63,65}\text{Cu}$  hyperfine splitting (Table 1). This is partly due to the solvent environment in  $[\text{Cu}(\text{L}^2)_2]$  and  $[\text{Cu}(\text{L}^3)_2]$  compared to the solid-state  $[\text{Ni}(\text{L}^1)_2]$  matrix<sup>17–19</sup> and is primarily due to the effects of ligand substituents in  $\text{L}^2$  (*t*-butyl;  $A_{\parallel} = -640$  MHz) and  $\text{L}^3$  (*t*-butyl and *N*-hexyl;  $A_{\parallel} = -620$  MHz). The spin Hamiltonian parameters are entirely consistent with a system possessing a square planar geometry with a  $d_{x^2-y^2}$  ground state.<sup>23</sup> Interestingly, the  $A_z$  ( $A_{\parallel}$ ) splitting of  $[\text{Cu}(\text{L}^3)_2]$  ( $-620$  MHz) is smaller compared to that of  $[\text{Cu}(\text{L}^2)_2]$  ( $-640$  MHz), once again indicating that the influence of the outer sphere hydrogen-bond-accepting  $-\text{CH}_2\text{N}(\text{C}_6\text{H}_{13})_2$  group is observable in the EPR spectrum.

**Q-Band  $^1\text{H}$  ENDOR.** The CW Q-band  $^1\text{H}$  ENDOR spectra for both  $[\text{Cu}(\text{L}^2)_2]$  and  $[\text{Cu}(\text{L}^3)_2]$  are shown in Figure 2 and

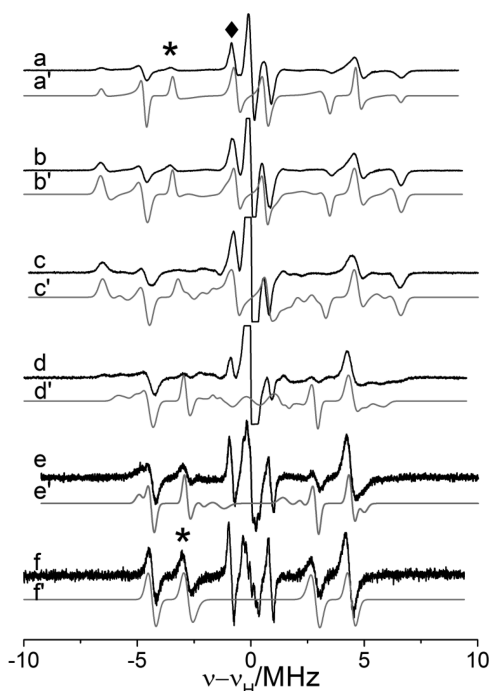


**Figure 2.** Q-band  $^1\text{H}$  ENDOR spectra (10 K) for  $[\text{Cu}(\text{L}^2)_2]$  recorded at the field positions (a) 1200.1, (b) 1195.5, (c) 1181.8, (d) 1144.1, (e) 1102.9, and (f) 1082.4 mT. Asterisk (\*) indicates that these labeled peaks arise from the  $A_1$  and  $A_3$  components of the hyperfine for the oxime proton ( $\text{H}^{16}$ ); the most likely peak associated with the remaining  $A_2$  component is marked with the  $\blacklozenge$  symbol. Corresponding simulations are shown, labeled a'–f'. The smaller coupling of 1.7 MHz, most clearly visible in f, likely arises from  $\text{H}^{11}$ .

Supporting Information Figure S1, respectively. The spectra were recorded over a range of magnetic field positions, ranging from 1080.0 to 1200.0 mT. This field range is necessary in order to extract the correct form of the  $^1\text{H}$ A tensor for an interacting ligand nucleus in the orientation-selective ENDOR experiment.<sup>24–27</sup> Improved resolution of the  $^1\text{H}$  resonances was obtained at Q-band frequencies since the large azomethine couplings (see below) were overlapped with the strongly coupled  $^{14}\text{N}$  signals in the X-band ENDOR spectra.

The  $^1\text{H}$  ENDOR spectra are dominated by hyperfine couplings from two strongly coupled protons, namely, the azomethine proton (labeled  $\text{H}^{15}$ ) and the H-bonded oxime proton (labeled  $\text{H}^{16}$ ), as shown in Scheme 2. These protons

were also clearly distinguished in the single-crystal ENDOR study of  $[\text{Cu}(\text{L}^1)_2]$ ,<sup>17</sup> where they were labeled  $\text{H}^{15}$  and  $\text{H}^{16}$ , respectively; for consistency, we have adopted the same labeling of these protons. The corresponding simulations for the two proton couplings are shown in Figure 2 (and Supporting Information Figure S2), and the resulting principal values of the hyperfine tensors are listed in Table 2. Analysis of the data

**Table 2.**  $^1\text{H}$  Principal Hyperfine Values for  $[\text{Cu}(\text{L}^1)_2]$ ,  $[\text{Cu}(\text{L}^2)_2]$ , and  $[\text{Cu}(\text{L}^3)_2]$ <sup>a</sup>

|  | $A_1$ <sup>b</sup> | $A_2$ <sup>c</sup> | $A_3$ <sup>b</sup> | $a_{\text{iso}}$ | $T_{\text{dip}}$ | $R/\text{\AA}$ <sup>d</sup> | ref       |
|--|--------------------|--------------------|--------------------|------------------|------------------|-----------------------------|-----------|
| $[\text{Cu}(\text{L}^1)_2]_{\text{sc}}$  |                    |                    |                    |                  |                  |                             |           |
| $\text{H}^{15}$                          | 13.00              | 9.15               | 8.48               | 10.21            | 2.79             | 3.97                        | 17        |
| $\text{H}^{16}$                          | 6.60               | -0.87              | -5.97              | -0.08            | 6.68             | 2.94                        | 17        |
| $[\text{Cu}(\text{L}^2)_2]_{\text{ply}}$ |                    |                    |                    |                  |                  |                             |           |
| $\text{H}^{15}$                          | 13.20              | 9.35               | 8.70               | 10.42            | 2.78             | 3.97                        | this work |
| $\text{H}^{16}$                          | 6.90               | -1.25              | -5.87              | -0.07            | 6.97             | 2.92                        | this work |
| $[\text{Cu}(\text{L}^3)_2]_{\text{ply}}$ |                    |                    |                    |                  |                  |                             |           |
| $\text{H}^{15}$                          | 12.7               | 9.30               | 8.70               | 10.23            | 2.47             | 4.13                        | this work |
| $\text{H}^{16}$                          | 6.90               | -1.25              | -4.00              | 0.55             | 3.65             | 3.01                        | this work |

<sup>a</sup>sc = single-crystal data; ply = polycrystalline toluene/dichloromethane frozen solution;  $T_{\text{dip}}$  is defined as the dipolar part of the  $^1\text{H}$  hyperfine coupling tensor ( $T_{\text{dip}} = A - a_{\text{iso}}$ ).  $A_1$ ,  $A_2$ , and  $A_3$  correspond to the  $A_x$ ,  $A_y$ , and  $A_z$  values referenced in refs 18 and 19. All hyperfine values are reported in MHz. <sup>b</sup>The errors in  $A$  for the polycrystalline measurements of  $[\text{Cu}(\text{L}^2)_2]_{\text{ply}}$  and  $[\text{Cu}(\text{L}^3)_2]_{\text{ply}}$  were  $\pm 0.1$ . <sup>c</sup>The errors in  $A$  for the polycrystalline measurements of  $[\text{Cu}(\text{L}^2)_2]_{\text{ply}}$  and  $[\text{Cu}(\text{L}^3)_2]_{\text{ply}}$  were  $\pm 0.2$ . <sup>d</sup>Errors in  $R = \pm 0.05$ . The Euler angles  $[\alpha, \beta, \gamma]$  are defined wrt the  $g$  tensor principal axis system. The Euler angles for  $[\text{Cu}(\text{L}^1)_2]_{\text{sc}}$  were reported as  $[180, 1.54, 157]$  for  $\text{H}^{15}$  and  $[101, 3.16, 143]$  for  $\text{H}^{16}$ . For the two polycrystalline samples, the Euler angles were all  $[0, 10, 0] \pm 10^\circ$  for  $\text{H}^{15}$  and  $\text{H}^{16}$ .

reveals that the azomethine protons ( $\text{H}^{15}$ ) are dominated by a large isotropic hyperfine coupling of  $a_{\text{iso}} = 10.42$  MHz in  $[\text{Cu}(\text{L}^2)_2]$  and  $a_{\text{iso}} = 10.23$  MHz in  $[\text{Cu}(\text{L}^3)_2]$ . The lower  $a_{\text{iso}}$  value in  $[\text{Cu}(\text{L}^3)_2]$  simply indicates a smaller unpaired spin density on  $\text{H}^{15}$ . It is worth mentioning briefly that the smaller coupling of 1.7 MHz observable in Figure 2f for  $[\text{Cu}(\text{L}^2)_2]$  likely arises from proton H11 (Scheme 2). According to the single-crystal ENDOR data for  $[\text{Cu}(\text{L}^1)_2]$ , proton H11 has a  $^1\text{H}$ A tensor of  $A_x = -1.26$ ,  $A_y = 1.78$ , and  $A_z = -1.89$  MHz, and considering this pair of peaks is absent in the ENDOR spectrum of  $[\text{Cu}(\text{L}^3)_2]$ , being replaced by the substituent, this assignment seems very plausible. However, as we are primarily interested in the  $^1\text{H}$  couplings from the azomethine and H-bonded oxime protons, we did not include these peaks in the ENDOR simulation or analysis.

In addition to these small differences in  $a_{\text{iso}}$ , the dipolar components of the  $^1\text{H}$  hyperfine tensors ( $T_{\text{dip}}$ ) were also found to be different, i.e., 2.78 versus 2.47 MHz for  $[\text{Cu}(\text{L}^2)_2]$  and  $[\text{Cu}(\text{L}^3)_2]$ , respectively. These  $T_{\text{dip}}$  values can be analyzed using a simple point-dipole approximation<sup>28</sup> to yield the resulting  $\text{Cu}\cdots\text{H}^{15}$  distances of  $3.97 \pm 0.05$  and  $4.13 \pm 0.05$  Å, respectively. This indicates that the  $X = -\text{CH}_2\text{N}(\text{C}_6\text{H}_{13})_2$  group in  $[\text{Cu}(\text{L}^3)_2]$  influences the structural properties of the complexes, in this case by altering both the  $\text{Cu}\cdots\text{H}^{15}$  distance and changing the Fermi contact term ( $a_{\text{iso}}$ ). It is important to note that the hyperfine tensor for this  $\text{H}^{15}$  azomethine proton in  $[\text{Cu}(\text{L}^2)_2]$  and  $[\text{Cu}(\text{L}^3)_2]$  is similar to that reported for  $[\text{Cu}(\text{L}^1)_2]$ , confirming that the small changes reported in Table 2 by modification of the ligand in  $[\text{Cu}(\text{L}^3)_2]$  are real and meaningful.

In the case of the  $H^{15}$  azomethine protons, all three components of the larger hyperfine values were visible in the  $^1H$  ENDOR spectra. Unfortunately, in the case of the H-bonded oxime proton ( $H^{16}$ ), only two components of the hyperfine coupling are clearly visible in the experimental ENDOR spectra (effectively, the experimental equivalents of  $A_1$  and  $A_3$ , labeled with an asterisk (\*) in Figure 2 and Supporting Information Figure S2). The third component of this tensor is expected to have a small value (peak labeled  $\blacklozenge$  in Figure 2) and is partly overlapped with other peaks in the central part of the ENDOR spectra. The reported principal values of the hyperfine tensor for  $H^{16}$  in  $[Cu(L^1)_2]$  are given in Table 2 with  $a_{iso} = -0.08$  MHz and  $Cu \cdots H^{16} = 2.94$  Å. Using this hyperfine tensor as a starting reference point, the ENDOR simulations were undertaken, and the resulting optimized values of the  $H^{16}$  hyperfine tensors for  $[Cu(L^2)_2]$  and  $[Cu(L^3)_2]$  are listed in Table 2. The error associated with the  $A_2$  value in both cases is obviously higher compared to the clearly resolved  $A_1$  and  $A_3$  components. Nevertheless, some important insights into the perturbation to this H-bonded oxime proton can be obtained using these experimental hyperfine values.

Analysis of the hyperfine tensor gives  $a_{iso} = -0.07$  MHz with  $T_{dip} = 6.97$  MHz for  $[Cu(L^2)_2]$ , and these values are found to be similar to those of the related  $[Cu(L^1)_2]$  complex (Table 2). By comparison, slightly different values of  $a_{iso} = 0.55$  MHz and  $T_{dip} = 3.65$  MHz were obtained for the  $[Cu(L^3)_2]$  complex. It should be noted that in our simulations the unresolved  $A_2$  component of the  $H^{16}$  hyperfine coupling was assigned a value of  $-1.25$  MHz for both complexes (as a peak appears at this resonance frequency in the spectra). Although the remote  $H^{11}$  protons in  $[Cu(L^1)_2]$  (Scheme 2) have a reported  $^1HA$  tensor of  $[-1.26, 1.78, -1.89$  MHz], and this should also be visible in  $[Cu(L^2)_2]$  (Figure 2), this proton is absent in  $[Cu(L^3)_2]$  (where it is replaced by the  $-CH_2N(C_6H_{13})_2$  group), but a resonance peak is still visible at ca. 1.25 MHz in the spectrum, adding confidence to our assignments from the simulations for  $H^{16}$ .

The larger  $a_{iso}$  value for  $[Cu(L^3)_2]$  indicates a higher unpaired spin density on this  $H^{16}$  proton, while the smaller dipolar  $A_{dip}$  value indicates a longer  $Cu \cdots H^{16}$  distance (3.01 Å) compared to 2.92 Å in  $[Cu(L^2)_2]$ . These results can be explained in terms of the influence of the  $-CH_2N(C_6H_{13})_2$  group in the complex, causing an asymmetric polarization of the unpaired spin density in the Cu(II) orbitals (manifested in the smaller  $^{Cu}A_{||}$  value of  $-620$  MHz and larger  $a_{iso}$  value for  $H^{16}$ ) and a lengthening of the  $Cu \cdots H^{16}$  distance. In other words, the unpaired Cu(II) spin density appears to be polarized toward the  $H^{16}$  proton (higher  $a_{iso}$ ) and away from the  $H^{15}$  proton (lower  $a_{iso}$ ) due to the  $-CH_2N(C_6H_{13})_2$  group in  $[Cu(L^3)_2]$ .

**Q-Band  $^{14}N$  ENDOR.** Further information on the distribution of electron spin density in the copper complexes can be obtained from the  $^{14}N$  ENDOR spectra. The Q-band  $^{14}N$  ENDOR spectra for  $[Cu(L^2)_2]$  and  $[Cu(L^3)_2]$  are shown in Figure 3 and Supporting Information Figure S3. The  $^{14}N$  hyperfine and quadrupole parameters were obtained by simulation of the angular-selective ENDOR spectra, and the resulting values are listed in Table 3. The  $^{14}N$  hyperfine tensor is nearly axially symmetric. It has been reported that the largest principal axis is oriented approximately along the Cu–N bond direction in the  $[Cu(L^1)_2]$  single crystal<sup>18,19</sup> and a structurally related  $[Cu(msal)_2]$  complex ( $msal = N$ -methyl-salicylideneimine),<sup>29</sup> with the principal axis of  $A_3(Q_3)$  (or  $A_2$ ) normal to

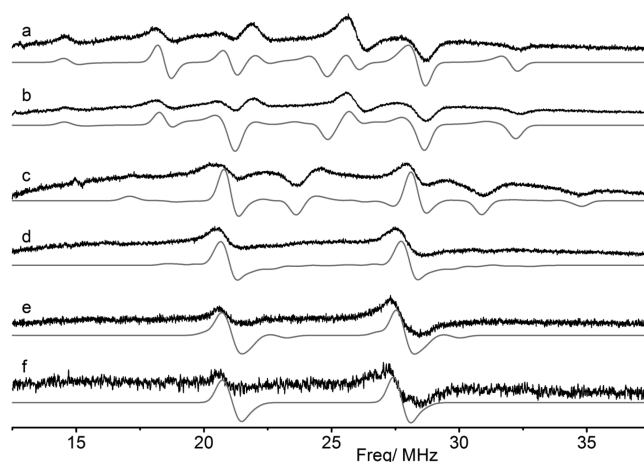


**Figure 3.** CW Q-band  $^{14}N$  ENDOR spectra (10 K) for  $[Cu(L^2)_2]$  recorded at the field positions (a) 1200.1, (b) 1195.5, (c) 1181.8, (d) 1144.1, (e) 1102.9, and (f) 1082.4 mT. Corresponding simulations are shown at each field position (gray line).

the complex plane (parallel to  $g_z$ ); we assumed that a similar orientation occurs in  $[Cu(L^2)_2]$  and  $[Cu(L^3)_2]$  in frozen solution (Table 3).

The hyperfine and quadrupole  $^{14}N$  values for  $[Cu(L^3)_2]$  are also listed in Table 3. Although the hyperfine values ( $^NA$ ) are similar compared to those of  $[Cu(L^2)_2]$ , changes are observed in the quadrupole values ( $^NQ$ ). This results in lower  $e^2qQ/h$  and asymmetry ( $\eta$ ) parameters (Table 3). The quadrupole parameter is very sensitive to changes in electron spin density in the plane of the Cu(II) complex, as variation occurs in the electric field gradient. So, in principle, subtle changes in spin redistribution in the  $d_{x^2-y^2}$  orbital caused by changes from the  $-CH_2N(C_6H_{13})_2$  functionality can be monitored. The changes to  $^NQ$ , particularly with the largest value changing from  $Q_2$  in  $[Cu(L^2)_2]$  to  $Q_1$  in  $[Cu(L^3)_2]$ , may be accounted for by the changes in spin polarization and further supports the observed trends found earlier via the  $^1H$  ENDOR data.

**DFT and X-ray Structure.** The above ENDOR data suggest that incorporation of an aminomethyl group ortho to the phenolic oxygen atom causes the length, and therefore strength, of the oxime-to-phenolate hydrogen bond to change significantly (evidenced by changes in  $Cu \cdots H$  distances). The extent to which these changes in the outer coordination sphere influence the structure and bonding in the inner sphere, and thus the strength of the ligands as copper extractants, is of considerable interest. To understand the origins of these substituent effects, we investigated the structure of the complexes by hybrid DFT calculations and X-ray crystallography. To reduce the numbers of possible conformers, the hybrid DFT calculations were performed on model complexes  $[Cu(L^4)_2]$  and  $[Cu(L^5)_2]$  that have methyl groups replacing the *t*-butyl and *n*-hexyl groups in  $[Cu(L^2)_2]$  and  $[Cu(L^3)_2]$ . The energy-minimized structure of  $[Cu(L^5)_2]$  *in vacuo* has the two aminomethyl groups displaced to the same side of the coordination plane (Figure 4). A more nearly centrosymmetric form with aminomethyl groups on opposite sides of the  $CuN_2O_2$  plane has a slightly higher energy (4.1 kJ mol), but it contains a similar arrangement of the H-bonds formed by the oximic hydrogen atoms ( $H^{16}$ ).

The changes in positions of the hydrogen atoms in the aminomethyl-substituted and unsubstituted compounds  $[Cu(L^5)_2]$  and  $[Cu(L^4)_2]$  mirror those found in the ENDOR

**Table 3.**  $^{14}\text{N}$  Hyperfine and Quadrupole Coupling Parameters for  $[\text{Cu}(\text{L}^1)_2]$ ,  $[\text{Cu}(\text{L}^2)_2]$ , and  $[\text{Cu}(\text{L}^3)_2]^a$ 

| solvent                                  | $A_1^b$ | $A_2$ | $A_3$ | $Q_1^c$ | $Q_2$ | $Q_3$ | $e^2qQ/h$ | $\eta$ |
|--|---------|-------|-------|---------|-------|-------|-----------|--------|
| $[\text{Cu}(\text{L}^1)_2]_{\text{sc}}$  | 51.96   | 42.10 | 43.64 | -1.71   | 1.91  | -0.20 | 3.82      | 0.79   |
| $[\text{Cu}(\text{L}^2)_2]_{\text{ply}}$ | 53.4    | 40.4  | 43.7  | -1.2    | 1.37  | -0.17 | 2.74      | 0.82   |
| $[\text{Cu}(\text{L}^3)_2]_{\text{ply}}$ | 53.0    | 39.8  | 44.1  | 1.1     | -0.92 | -0.2  | 1.84      | 0.67   |

<sup>a</sup>sc = single-crystal data; ply = polycrystalline toluene/dichloromethane frozen solution; all hyperfine and quadrupole values are reported in MHz. <sup>b</sup> $A$  values  $\pm 0.2$  MHz. <sup>c</sup> $Q$  values  $\pm 0.1$  MHz. Euler angles =  $[30, 10, 30] \pm 10^\circ$ . The Euler angles are defined wrt the  $g$  tensor principal axis system.  $A_1$ ,  $A_2$ , and  $A_3$  correspond to the  $A_x$ ,  $A_y$ , and  $A_z$  notations referenced in refs 18 and 19.

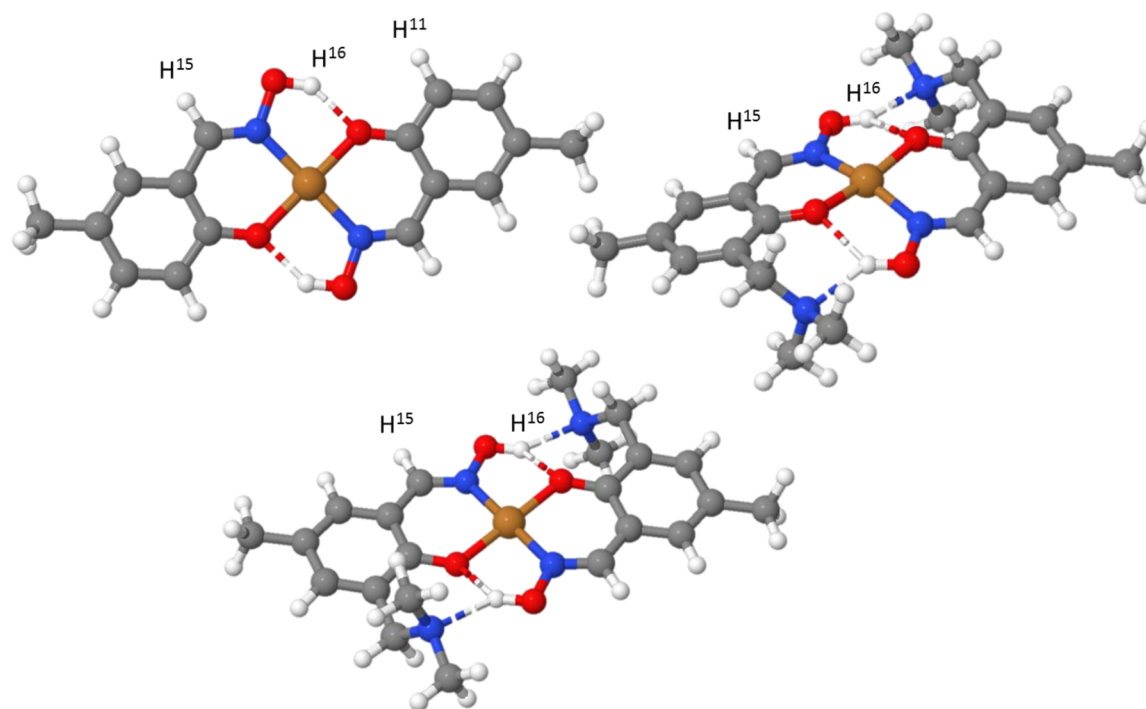


**Figure 4.** Energy-minimized structures of  $[\text{Cu}(\text{L}^4)_2]$  and  $[\text{Cu}(\text{L}^5)_2]$  (top), showing contacts made by the oximic hydrogen atoms. The slightly higher energy, centrosymmetric form of  $[\text{Cu}(\text{L}^5)_2]$  (bottom) is included for comparison. Nitrogen, oxygen, and copper atoms are colored blue, red, and brown, respectively.

studies of  $[\text{Cu}(\text{L}^3)_2]$  and  $[\text{Cu}(\text{L}^2)_2]$ . In particular, the interaction of the  $\text{H}^{16}$  atom with the amine nitrogen atom causes it to move away from the central copper atom (Table 4; increased  $\text{Cu}\cdots\text{H}$  distance). This movement is accompanied by a shortening of the  $\text{Cu}-\text{O}$  bonds and a lengthening of the  $\text{Cu}-$

**Table 4.** Interatomic Distances ( $\text{\AA}$ ) from ENDOR Measurements, Hybrid DFT Calculations, and Single-Crystal X-ray Structure Determinations

|                             | $\text{Cu}\cdots\text{H}^{15}$ | $\text{Cu}\cdots\text{H}^{16}$ | $\text{Cu}-\text{O}$ | $\text{Cu}-\text{N}$ |
|-----------------------------|--------------------------------|--------------------------------|----------------------|----------------------|
|                             |                                | ENDOR/ $\text{\AA}$            |                      |                      |
| $[\text{Cu}(\text{L}^2)_2]$ | 3.97                           | 2.92                           |                      |                      |
| $[\text{Cu}(\text{L}^3)_2]$ | 4.13                           | 3.01                           |                      |                      |
|                             |                                | hybrid DFT/ $\text{\AA}$       |                      |                      |
| $[\text{Cu}(\text{L}^4)_2]$ | 3.92                           | 2.60                           | 1.93                 | 1.96                 |
| $[\text{Cu}(\text{L}^5)_2]$ | 3.94                           | 2.96                           | 1.89                 | 2.00                 |
|                             |                                | XRD/ $\text{\AA}$              |                      |                      |
| $[\text{Cu}(\text{L}^2)_2]$ | $3.77^{a,c}$                   | $2.71^{a,c}$                   | $1.904(2)^a$         | $1.943(2)^a$         |
| $[\text{Cu}(\text{L}^6)_2]$ | $3.77^{b,c}$                   | $2.83^{b,c}$                   | $1.896(1)^b$         | $1.958(2)^b$         |

<sup>a</sup>Average of three crystallographically independent values. <sup>b</sup>Average of two crystallographically independent values present in metal complex dimer  $[\text{Cu}(\text{L}^6)_2]_2$  (see Figure 5). <sup>c</sup>No SD values for positional parameters are provided for H atoms in these structures. <sup>9,11</sup>

$\text{N}$  bonds, and, as a consequence, the azomethine hydrogen atom  $\text{H}^{15}$  becomes more remote from the copper atom, as revealed by the ENDOR spectra.

The strengths of the H-bonds in  $[\text{Cu}(\text{L}^4)_2]$  and  $[\text{Cu}(\text{L}^5)_2]$  were also compared using natural bond order (NBO) calculations. The bond between the oximic hydrogen and the phenolate oxygen atoms in the unsubstituted compound  $[\text{Cu}(\text{L}^4)_2]$  is considerably stronger (39 kJ/mol) compared to that in  $[\text{Cu}(\text{L}^5)_2]$  (19 kJ/mol) (see Supporting Information Figures S4 and S5), presumably because the amine group in the latter is competing for the H-bond donor (22 kJ/mol).

The effects of aminomethyl group substitution in the 3-position on the structures of complexes in the solid state were evaluated by comparing the single-crystal X-ray structures of  $[\text{Cu}(\text{L}^2)_2]$ <sup>9</sup> and  $[\text{Cu}(\text{L}^6)_2]$ <sup>12</sup> (Figure 5). The aminomethyl group in the latter complex contains a relatively rigid piperidine unit, which facilitated the isolation of good quality single crystals.<sup>11</sup> The distortion of the  $\text{CuN}_2\text{O}_2$  coordination geometry from planarity in  $[\text{Cu}(\text{L}^6)_2]$  is similar to that observed in the calculated structure of  $[\text{Cu}(\text{L}^5)_2]$  (Figure 4) and is enhanced by the formation of a dinuclear complex through an interaction of one phenolate oxygen atom with the Cu atom in a neighboring complex (Figure 5, right). As in the DFT structures, the  $\text{Cu}-\text{N}$  bonds are longer in the amine-

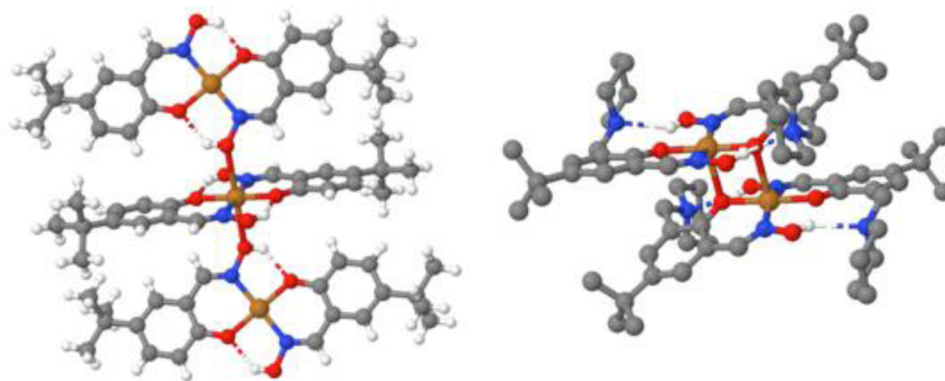


**Figure 5.** Part of the X-ray crystal structure of  $[\text{Cu}(\text{L}^2)_2]$  and a view of the  $[\text{Cu}(\text{L}^6)_2]$  dimer. For clarity, hydrogen atoms attached to carbon have been omitted from the latter.

substituted complex (1.958(2) cf. 1.943(3) Å; Table 4), and this likely explains the observed differences in the  $^{\text{N}}\text{A}$  and  $^{\text{N}}\text{Q}$  values observed by ENDOR. The differences between the averaged Cu–O lengths follow the variations predicted by the DFT calculations but are barely statistically significant, possibly as a consequence of the phenolate groups in each solid-state structure having different environments. In each structure, one phenolate oxygen atom forms a weak bond to a copper atom in an adjacent complex, forming a dinuclear complex in the case of  $[\text{Cu}(\text{L}^6)_2]$  and a polynuclear array in  $[\text{Cu}(\text{L}^2)_2]$  (Figure 5).

Using the X-ray crystal structures of  $[\text{Cu}(\text{L}^2)_2]$  and  $[\text{Cu}(\text{L}^6)_2]$  to follow the effects of substitution on differences in the positions of the oximic hydrogen ( $\text{H}^{16}$ ) atoms is difficult because the published structure has these atoms in calculated positions riding on their attached oxygen atoms. Consequently, the apparent lengthening of the  $\text{Cu}\cdots\text{H}^{16}$  distance in the buttressed complex  $[\text{Cu}(\text{L}^6)_2]$  associated with  $\text{H}^{16}$  being pulled toward the amine group (Table 4) is not statistically significant. However, it is possible to track the movement of the oximic oxygen atom away from the copper toward the aminomethyl group in  $[\text{Cu}(\text{L}^6)_2]$  (see Supporting Information Figure S4). The mean  $\text{Cu}\cdots\text{O}_{\text{oxime}}$  distance in  $[\text{Cu}(\text{L}^6)_2]$  is 2.923(2) cf. 2.855(2) Å in  $[\text{Cu}(\text{L}^2)_2]$ , which is consistent with results from the ENDOR and DFT studies above. While the magnitude of the variations of the lengths in Table 4 resulting from the introduction of a 3-dialkylaminomethyl substituent are not comparable for the reasons mentioned, the trends are the same, regardless of whether the structure is determined in solution or in the gas or solid state.

As mentioned above, the incorporation of substituents ortho to the phenol group has been shown to have a major effect on their strength as Cu extractants in the pH-dependent equilibrium. Copper extractions by chloroform solutions of  $\text{L}^2\text{H}$  and  $\text{L}^3\text{H}$  are presented in Figure 6 and compared with the strongest of a series of salicylaldoxime extractants (the 3-bromo-substituted  $\text{L}^9\text{H}$ ) and the weakest (the 3-*t*-butyl-substituted  $\text{L}^{10}\text{H}$ ). The 3-aminomethyl-substituted extractant  $\text{L}^3\text{H}$  is only slightly stronger than the unsubstituted reagent,  $\text{L}^2\text{H}$ , having a  $\text{pH}_{0.5}$  value (the pH for 50% metal loading) of 1.45. At first sight, this is surprising, given the strong buttressing H-bond in  $[\text{Cu}(\text{L}^3)_2]$  that has been demonstrated above, and the observation that such buttressing is the dominant factor in determining the relative strengths of the eight extractants studied previously.<sup>9</sup> The anomalous behavior of the 3-aminomethyl substituent in  $\text{L}^3\text{H}$  can be understood by using hybrid DFT calculations to compare substituent effects

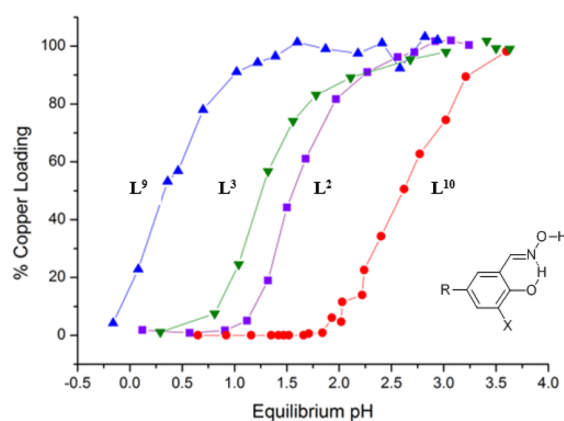
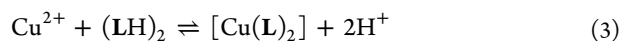


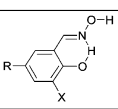
**Figure 6.** pH profiles for copper extraction by 0.01 M chloroform solutions of  $\text{L}^2\text{H}$ ,  $\text{L}^3\text{H}$ ,  $\text{L}^9\text{H}$ , and  $\text{L}^{10}\text{H}$  from equal volumes of 0.01 M aqueous solutions of  $\text{CuSO}_4$ ; 100% loading represents Cu uptake corresponding to formation of a 1:2 complex  $\text{CuL}_2$ .

on the deprotonation energies of the proligands ( $\Delta U_{\text{dp}}$ , eq 1), the binding energies of the anionic ligands to  $\text{Cu}^{2+}$  ( $\Delta U_{\text{b}}$ , eq 2), and the formation energies of the copper complexes (eq 3,  $\Delta U_{\text{f}} = \Delta U_{\text{dp}} + \Delta U_{\text{b}}$ ).



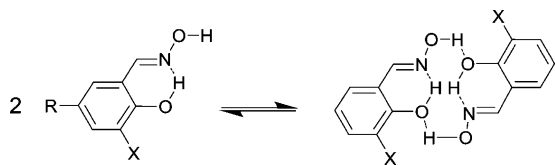
The calculated formation energies of the Cu complexes ( $\Delta U_{\text{f}}$ , Table 5) are increasingly favorable in the order  $\text{L}^8\text{H} < \text{L}^5\text{H} < \text{L}^4\text{H} < \text{L}^7\text{H}$  (i.e., as the X substituent is changed from *t*-Bu to  $\text{CH}_2\text{-N-morpholine}$  to H and to Br). The bromo-substituted reagent,  $\text{L}^7\text{H}$ , is predicted to be the strongest extractant because it has the lowest deprotonation energy ( $\Delta U_{\text{dp}}$ ) and the second most favorable interligand hydrogen bonding, as revealed by the dimerization energies ( $\Delta U_{\text{dim}}$ ). The former can be ascribed to the electron-withdrawing properties of the bromine, and the latter is consistent with some form of additional intracomplex secondary bonding, such as buttressing of the H-bonding,<sup>9</sup> that contributes to the stability of the Cu complex. These terms, which favor complex formation, more than compensate for the weaker binding energy to Cu(II) that

**Table 5.** Calculated Dimerization (eq 4), Deprotonation (eq 1), Binding (eq 2), and Complex Formation Energies (eq 3)

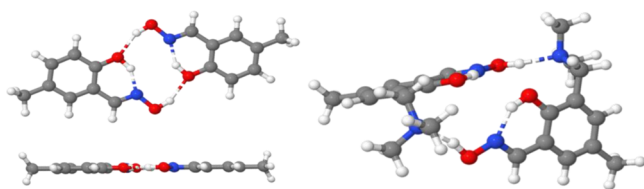
| LH  |  | $\Delta U_{\text{dim}}$ | $\Delta U_{\text{dp}}$ | $\Delta U_{\text{b}}$ | $\Delta U_{\text{f}}$ |
|---|--|-------------------------|------------------------|-----------------------|-----------------------|
|   |  | /kJ mol <sup>-1</sup>   | /kJ mol <sup>-1</sup>  | /kJ mol <sup>-1</sup> | /kJ mol <sup>-1</sup> |
|  | X  |                         |                        |                       |                       |
| L <sup>4</sup> H  | H  | -40.4                   | 3031.0                 | -2897.2               | 133.8                 |
| L <sup>5</sup> H  | CH <sub>2</sub> N(CH <sub>3</sub> ) <sub>2</sub> | -73.4                   | 3053.5                 | -2905.4               | 148.1                 |
| L <sup>7</sup> H  | Br   | -44.8                   | 2969.5                 | -2843.3               | 126.2                 |
| L <sup>8</sup> H  | <sup>t</sup> Bu                                  | -28.8                   | 3000.8                 | -2830.3               | 170.5                 |

arises from the bromo-substituent reducing the basicity of the N<sub>2</sub>O<sub>2</sub><sup>2-</sup> donor set.

The ENDOR, hybrid DFT, and X-ray structural data above all indicate that the aminomethyl substituent ortho to the phenolic oxygen atom provides particularly strong buttressing of interligand H-bonding. This is manifested by L<sup>5</sup>H having the most favorable dimerization energy ( $\Delta U_{\text{dim}}$ ; Table 5) for the process shown in Figure 7 and eq 4. While the buttressed H-

**Figure 7.** Dimerization to give the proligands with preorganized N<sub>2</sub>O<sub>2</sub> donor sets.

bonding is very favorable in the proligand dimer [L<sup>5</sup>H]<sub>2</sub> in the gas phase, it preorganizes the N<sub>2</sub>O<sub>2</sub> donor set to give a nonplanar arrangement (Figure 8), which is a poor fit for

**Figure 8.** Energy-minimized structures of the proligand dimers [L<sup>4</sup>H]<sub>2</sub> and [L<sup>5</sup>H]<sub>2</sub>, contrasting the planar preorganization of the N<sub>2</sub>O<sub>2</sub> donor set in [L<sup>4</sup>H]<sub>2</sub> (left) and the nonplanar arrangement in [L<sup>5</sup>H]<sub>2</sub> (right).

Cu(II). Consequently, the binding energy to Cu(II) ( $\Delta U_{\text{b}}$ ) is smaller than that in the unsubstituted reagent L<sup>4</sup>H and does not compensate for its high deprotonation energy.

The combination of techniques described above has demonstrated that buttressing the H-bonding in the outer coordination sphere of extracted metal complexes significantly influences their structures and stabilities. However, the work also reveals that it will not always be the case that reagents which provide the strongest buttressing will prove to be the strongest extractants; the buttressing may impose an unfavorable coordination geometry on the complexed metal.

## CONCLUSIONS

EPR and ENDOR spectroscopy at two different frequencies, used to investigate Cu(II) complexes bearing 3-X-salicylaldoximes in frozen solution, provide information for the first time

on the relative strengths of hydrogen bonds formed in a medium/environment that is similar to that used in commercial solvent extraction processes. This information is important because the selectivity and strength of copper extraction are known to be dependent on interligand H-bonding.<sup>3a</sup>

The *g* and <sup>63</sup>Cu spin Hamiltonian parameters extracted by simulation of the EPR spectra confirm the square planar geometry of the complexes, and the observed values were found to be in close agreement with the reported values for the unsubstituted doped single crystal of [Cu(L<sup>1</sup>)<sub>2</sub>].<sup>17</sup> Analysis of the Q-band <sup>1</sup>H and <sup>14</sup>N ENDOR data reveal an asymmetric spin polarization of the unpaired electron caused by the peripheral -CH<sub>2</sub>N(C<sub>6</sub>H<sub>13</sub>)<sub>2</sub> groups in [Cu(L<sup>3</sup>)<sub>2</sub>]. This is manifest through a higher *a*<sub>iso</sub> value for the oxime H<sup>16</sup> atom and a lower *a*<sub>iso</sub> value for the azomethine H<sup>15</sup> atom compared to those of [Cu(L<sup>2</sup>)<sub>2</sub>]. Crucially, the Cu⋯H<sup>16</sup> distance was found to be noticeably longer in [Cu(L<sup>3</sup>)<sub>2</sub>] than in [Cu(L<sup>2</sup>)<sub>2</sub>], as determined from the dipolar component of the <sup>1</sup>H hyperfine tensor using the point dipole approximation. This can be interpreted in terms of a weaker H-bond between the oxime proton (H<sup>16</sup>) and the coordinated phenolate oxygen in [Cu(L<sup>3</sup>)<sub>2</sub>], resulting from polarization of the H<sup>16</sup> proton toward the -CH<sub>2</sub>N(C<sub>6</sub>H<sub>13</sub>)<sub>2</sub> group. These changes in interligand H-bonding, arising from the introduction of an aminomethyl group, are mirrored in the structures of closely related model complexes obtained in the gas phase by DFT calculations and in the solid state by X-ray structure determination. The hyperfine tensor for the H<sup>15</sup> azomethine proton in [Cu(L<sup>2</sup>)<sub>2</sub>] and [Cu(L<sup>3</sup>)<sub>2</sub>] is similar to that reported for [Cu(L<sup>1</sup>)<sub>2</sub>]. Although the *magnitudes* of the changes in contact distances and bond lengths caused by the incorporation of the buttressing 3-X groups are not the same in solution or in the gas phase and solid states for the reasons presented above, the *trends* are the same in all cases.

Earlier work suggested that the ability of 3-X-substituents in salicylaldoximes to buttress the H-bonding between ligands in the outer coordination sphere is the dominant effect in determining their strength as copper extractants. In this Article, the combination of structural investigations and DFT calculations of energies of formation for the copper complexes has revealed that this is not always the case. The very strong additional (buttressing) H-bonds formed by aminomethyl substituents do not greatly increase the strength of copper extraction because they impose an unfavorable geometry on the complexed metal. These substituents also increase the energy required to deprotonate the extractant and thereby form the neutral complexes with Cu(II).

## ASSOCIATED CONTENT

### Supporting Information

The Supporting Information is available free of charge on the ACS Publications website at DOI: 10.1021/acs.inorgchem.5b01180.

Q-band <sup>1</sup>H ENDOR spectra of [Cu(L<sup>3</sup>)<sub>2</sub>], comparative Q-band <sup>1</sup>H ENDOR spectra of [Cu(L<sup>3</sup>)<sub>2</sub>] and [Cu(L<sup>2</sup>)<sub>2</sub>], Q-band <sup>14</sup>N ENDOR spectra of [Cu(L<sup>3</sup>)<sub>2</sub>], calculated and found intramolecular Cu⋯O<sub>oxime</sub> and O<sub>phenol</sub>⋯O<sub>oxime</sub> distances and NBO-calculated energies of H-bonds formed by the oxime H<sup>16</sup> in selected complexes and proligand dimers, and Cartesian coordinates for all energy-minimized structures (PDF).



## AUTHOR INFORMATION

## Corresponding Authors

\* (D.M.M.) E-mail: [MurphyDM@cardiff.ac.uk](mailto:MurphyDM@cardiff.ac.uk)

\* (P.A.T.) E-mail: [P.A.Tasker@ed.ac.uk](mailto:P.A.Tasker@ed.ac.uk)

## Notes

The authors declare no competing financial interest.

## ACKNOWLEDGMENTS

We thank the EPSRC and Cytec Industries for funding Ph.D. studentships for R.S.F., R.J.G., and M.R.H. as well as for PDRA funding for E.C., the EaStCHEM research computing facility for access to software, and the Edinburgh Computer and Data Facilities (ECDF) for access to hardware.

## REFERENCES

- (1) Hamilton, J. A.; Sabesan, M. N.; Steinrauf, L. K. *J. Am. Chem. Soc.* **1981**, *103*, 5880–5885.
- (2) Godycki, L. E.; Rundle, R. E. *Acta Crystallogr.* **1953**, *6*, 487–495.
- (3) (a) Turkington, J. R.; Bailey, P. J.; Love, J. B.; Wilson, A. M.; Tasker, P. A. *Chem. Commun.* **2013**, *49*, 1891. (b) Wilson, A. M.; Bailey, P. J.; Tasker, P. A.; Turkington, J. R.; Grant, R. A.; Love, J. B. *Chem. Soc. Rev.* **2014**, *43*, 123–134.
- (4) (a) Tasker, P. A.; Pliieger, P. G.; West, L. C. *Comprehensive Coordination Chemistry II* **2003**, *9*, 759–808. (b) Nicol, M. J.; Fleming, C. A.; Preston, J. S. *Comprehensive Coordination Chemistry* **1987**, *6*, 779–842.
- (5) (a) Brammer, L. *Dalton Trans.* **2003**, *16*, 3145–3287. (b) Belkova, N. V.; Shubina, E. S.; Epstein, L. M. *Acc. Chem. Res.* **2005**, *38*, 624–631. (c) Grabowski, S. J. *Chem. Rev.* **2011**, *111*, 2597–2625.
- (6) (a) Cole, P. M.; Sole, K. C.; Feather, A. M. *Tsinghua Sci. Technol.* **2006**, *11*, 153–159. (b) Sole, K. C.; Feather, A. M.; Cole, P. M. *Hydrometallurgy* **2005**, *78*, 52–78.
- (7) Szymanowski, J. *Hydroxyoximes and Copper Hydrometallurgy*; CRC Press: Boca Raton, FL, 1993.
- (8) (a) Mackey, P. J. *CIM Magazine* **2007**, *2*, 35. (b) Kordosky, G. A. International Solvent Extraction Conference, Cape Town, South Africa, March 17–21, 2002, p 853.
- (9) Forgan, R. S.; Roach, B. D.; Wood, P. A.; White, F. J.; Campbell, J.; Henderson, D. K.; Kamenetzky, E.; McAllister, F. E.; Parsons, S.; Pidcock, E.; Richardson, P.; Swart, R. M.; Tasker, P. A. *Inorg. Chem.* **2011**, *50*, 4515–4522.
- (10) Smith, A. G.; Tasker, P. A.; White, D. J. *Coord. Chem. Rev.* **2003**, *241*, 61–85.
- (11) Forgan, R. S.; Davidson, J. E.; Fabbiani, F. P. A.; Galbraith, S. G.; Henderson, D. K.; Moggach, S. A.; Parsons, S.; Tasker, P. A.; White, F. J. *Dalton Trans.* **2010**, *39*, 1763–1770.
- (12) Stoll, S.; Schweiger, A. *J. Magn. Reson.* **2006**, *178*, 42–55.
- (13) Frisch, M. J.; Trucks, G. W.; Schlegel, H. B.; Scuseria, G. E.; Robb, M. A.; Cheeseman, J. R.; Scalmani, G.; Barone, V.; Mennucci, B.; Petersson, G. A.; Nakatsuji, H.; Caricato, M.; Li, X.; Hratchian, H. P.; Izmaylov, A. F.; Bloino, J.; Zheng, G.; Sonnenberg, J. L.; Hada, M.; Ehara, M.; Toyota, K.; Fukuda, R.; Hasegawa, J.; Ishida, M.; Nakajima, T.; Honda, Y.; Kitao, O.; Nakai, H.; Vreven, T.; Montgomery, J. A., Jr.; Peralta, J. E.; Ogliaro, F.; Bearpark, M.; Heyd, J. J.; Brothers, E.; Kudin, K. N.; Staroverov, V. N.; Kobayashi, R.; Normand, J.; Raghavachari, K.; Rendell, A.; Burant, J. C.; Iyengar, S. S.; Tomasi, J.; Cossi, M.; Rega, N.; Millam, J. M.; Klene, M.; Knox, J. E.; Cross, J. B.; Bakken, V.; Adamo, C.; Jaramillo, J.; Gomperts, R.; Stratmann, R. E.; Yazyev, O.; Austin, A. J.; Cammi, R.; Pomelli, C.; Ochterski, J. W.; Martin, R. L.; Morokuma, K.; Zakrzewski, V. G.; Voth, G. A.; Salvador, P.; Dannenberg, J. J.; Dapprich, S.; Daniels, A. D.; Farkas, O.; Foresman, J. B.; Ortiz, J. V.; Cioslowski, J.; Fox, D. J. *Gaussian 09*, revision D.01; Gaussian, Inc.: Wallingford, CT, 2009.
- (14) Glendenning, D.; Badenhop, J. K.; Reed, A. E.; Carpenter, J. E.; Bohmann, J. A.; Morales, C. M.; Weinhold, F. *NBO 5.G*; Theoretical Chemistry Institute, University of Wisconsin: Madison, WI, 2001.
- (15) (a) Becke, A. D. *J. Chem. Phys.* **1993**, *98*, 5648–5652. (b) Lee, C.; Yang, W.; Parr, R. G. *Phys. Rev. B: Condens. Matter Mater. Phys.* **1988**, *37*, 785–789.
- (16) Boys, S. F.; Bernardi, F. *Mol. Phys.* **1970**, *19*, 553–566.
- (17) Schweiger, A. *Struct. Bonding (Berlin)* **1982**, *51*, 1.
- (18) Schweiger, A.; Gunthard, Hs.H. *Chem. Phys.* **1978**, *32*, 35–61.
- (19) Schweiger, A.; Rist, G.; Gunthard, Hs.H. *Chem. Phys. Lett.* **1975**, *31*, 48–52.
- (20) (a) McCudden, B.; O'Brien, P.; Thornback, J. R. *J. Chem. Soc., Dalton Trans.* **1983**, 2043–2046. (b) O'Brien, P.; Thornback, J. R.; Szymamowski, J. *J. Coord. Chem.* **1983**, *13*, 11–15.
- (21) Ovchinnikov, I. V.; Konstantinov, V. N. *J. Magn. Reson.* **1978**, *32*, 179–190.
- (22) Mabbs, F. E.; Collison, D. *Electron Paramagnetic Resonance of d Transition Metal Compounds*; Elsevier: New York, 1992.
- (23) Pilbrow, J. R. *Transition Ion Electron Paramagnetic Resonance*; Oxford University Press: Oxford, 1990.
- (24) Rist, G. H.; Hyde, J. S. *J. Chem. Phys.* **1970**, *52*, 4633–4643.
- (25) (a) Hoffman, B. M.; Martinsen, J.; Venters, J. *J. Magn. Reson.* **1984**, *59*, 110–123. (b) Hoffman, B. M.; Venters, J.; Martinsen, J. *J. Magn. Reson.* **1985**, *62*, 537–542.
- (26) (a) Hurst, G. C.; Henderson, T. A.; Kreilick, R. W. *J. Am. Chem. Soc.* **1985**, *107*, 7294–7299. (b) Henderson, T. A.; Hurst, G. C.; Kreilick, R. W. *J. Am. Chem. Soc.* **1985**, *107*, 7299–7303.
- (27) Murphy, D. M.; Farley, R. D. *Chem. Soc. Rev.* **2006**, *35*, 249–268.
- (28) Attanasio, D. *J. Phys. Chem.* **1986**, *90*, 4952–4957.
- (29) Moores, B. W.; Belford, R. L. *Electron Spin Resonance of Metal Complexes*; Yen, T. F., Ed.; Plenum Press: New York, 1969; p 13.